Computer Project 1: Accuracy, Stability, Convergence for Linear Advection and Ideal MHD Plasma Model

Peter Preisler
University of Washington, 98105, USA
(Dated: April 28, 2025)

This paper explores five different numerical schemes that are used to analyze the linear advection equation: Forward Time Backward Space (FTBS), Forward Time Center Space (FTCS), Lax-Friedrichs (LF), Lax-Wendroff (LW), and Runge Kutta together with a Centered Finite Difference scheme (RK). All algorithms are studied mathematically using truncation-error expansion and Von Neumann stability analysis, to find their accuracy and determine their stability. The FTCS and RK algorithm are found to be unconditionally unstable, while the other three are stable under suitable conditions. The numerical simulations show that the character of the numerical error is shaped by the order of the dominant spatial derivative. Here, the LW scheme shows the highest accuracy with a dominant dispersive error. Finally, the LF scheme is generalized to simulate the 1D ideal-MHD model and solve the Brio-Wu shock problem. The results from the corresponding paper are successfully reproduced.

INTRODUCTION

This project explores different numerical methods for solving the linear advection equation

$$\frac{\partial u}{\partial t} + a\frac{\partial u}{\partial x} = 0, \tag{1}$$

where a is a constant, set to 1 for the purpose of this project. The equation describes the transport of a quantity $u(x,t)$ with a constant velocity a.

In total, five different numerical schemes are studied for their accuracy and stability properties. For this, analytical, as well as numerical solutions are obtained and compared. The following list of algorithms includes their names as well the explicit mathematical formulation. Here, n denotes the time step and j the position in space at which u is evaluated:

1. Forward Time Backward Space (FTBS)
2. Forward Time Centered Space (FTCS)
3. Lax-Friedrichs (LF)
4. Lax-Wendroff (LW)
5. Runge-Kutta 2nd order & CFD 4th order (RK)

Analytically, the numerical scheme's accuracy is evaluated by determining the local truncation error τ. The stability analysis, on the other hand, makes use of a transformation into wave number space to yield a stability condition according to Von Neumann's method.

For the simulation, a one dimensional domain extending from $x = 0$ to $x = \pi$ is used. This domain is periodically closed, meaning that $u(0,t) = u(\pi,t)$ for all t. Moreover, the domain is initialized with two different waveforms. For one, a square wave that is equal to 1 for $\frac{\pi}{4} \leq x \leq \frac{\pi}{2}$ and for the other, a squared sine wave.

Lastly, the Lax-Friedrichs algorithm is generalized to describe the 1D MHD equations and solve them. In particular, the simulation domain and initial conditions are chosen equal to the ones in [1], leading to the construction of the Brio-Wu shock problem. The results of the simulation exactly match the results from the paper and demonstrate how powerful the discussed numerical schemes are to solve physical problems.

ALGORITHM ANALYSIS & COMPARISON

In this section, the five introduced algorithms are analytically and numerically analyzed and compared to each other. This shall give a good understanding of the pros and cons of the different numerical schemes.

Forward Time Backward Space

As a start, the most basic of all algorithms is explored since it gives a good feeling for the concept of Finite Difference Methods (FDM). This algorithm discretizes a single derivative with the slope of two neighboring points in the simulation domain.

$$\frac{\partial u}{\partial t} \approx \frac{u_j^{n+1} - u_j^n}{\Delta t}, \tag{2}$$

$$\frac{\partial u}{\partial x} \approx \frac{u_j^n - u_{j-1}^n}{\Delta x}. \tag{3}$$

To find an expression for the next time step in the future, we have to use a forward step in time (Forward Euler). For space, however, we could use a step to the left, or to the right of the current position. In this case, we chose $a = 1$, so the wave will move towards positive x values in time. Thus, it makes sense to define a backward facing derivative. Plugging these approximations into the PDE

given above, we can rearrange the equation to get:

$$\tilde{u}_j^{n+1} = u_j^n - \frac{a\Delta t}{\Delta x}(u_j^n - u_{j-1}^n). \tag{4}$$

With this explicit scheme, we can use the known quantities at time n, to calculate the function values in the next time step $n+1$.

Since the finite differences are only approximations, $\tilde{u}_j^{n+1}$ is not exactly equal to the *real* next time step u_j^{n+1}. This leads to the definition of the local truncation error

$$\tau = \frac{u_j^{n+1} - \tilde{u}_j^{n+1}}{\Delta t}.$$

By expressing both u_j^{n+1}, and the quantities u_j^n and u_{j-1}^n as Taylor expansions, one can derive the accuracy of the numerical method by collecting the lowest order Δt and Δx terms of τ. The explicit calculation is performed in the appendix and leads to equation 13 that determines the accuracy of the FTBS scheme to be first order in time and space.

The stability analysis relies on the definition of the error $\varepsilon_j^n = \tilde{u}_j^{n+1} - u_j^{n+1}$, that describes the difference between the approximate and real solution. This error also fulfills equation 4. Assuming wave behavior we can transform into Fourier space, where the error can be described as

$$\varepsilon_j^n = V^n e^{ikj\Delta x}, \tag{5}$$

where V^n is the wave amplitude for a given time step and k is the wave number. For stability, the wave amplitude of two consecutive time steps must not grow. This leads to the Von Neumann stability condition

$$|G| = \left|\frac{V^{n+1}}{V^n}\right| \leq 1. \tag{6}$$

Inserting equation 5 into the PDE, will lead to an expression for $|G|$. This will usually restrict the so called CFL number $\nu = \frac{a\Delta t}{\Delta x}$, that combines all decisive quantities for a given simulation. Thus, stability cannot be ensured by limiting the grid size in one dimension, but results from the relative grid size in terms of time and space. For the FTBS scheme, the numerical stability is ensured for $0 \leq \nu \leq 1$ (see 14).

Interestingly, the stability analysis of a forward time forward space algorithm will lead to stability in the range $-1 \leq \nu \leq 0$ (while $a = 1$). This can only be achieved with a negative value for a, i.e. a change of the PDE itself. In other words: the decision for forward or backward steps in time should be made depending on the value of the wave speed of the given PDE.

The numerical simulations for all stable schemes are presented on a 3x3 grid that shows the simulation domain for different grid spacings $\Delta x = \frac{\pi}{N_x}$ and different CFL numbers ν. For every combination of those parameters, both the square and the squared sine wave are plotted.

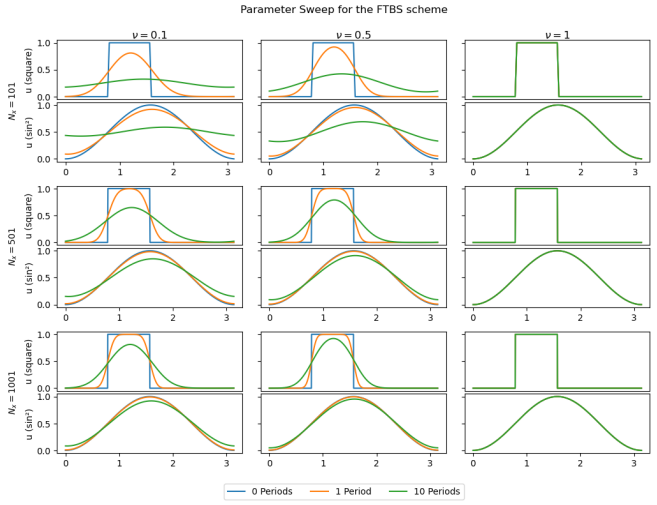

Figure 1. This figure shows the numerical behavior of the simulation domain for the FTBS scheme. It shows the solutions over time and for different combinations of N_x and ν.

To show the evolution over time, each wave is depicted at three times. At initialization, after 1 period, and after 10 periods. Figure 1 shows the simulations for the FTBS algorithm. This, and all other plots can also be found at a bigger scale version in the project's jupyter notebook that serves as an appendix to this paper.

The simulations show the following behavior:

- Agreement with the stability analysis: shows unstable behavior for CFL numbers smaller than 0 or larger than 1.
- CFL = 1 leads to almost perfect result; shape and period preserved.
- Smaller CFL numbers lead to a loss of shape; especially the square wave becomes rounded off.
- Smaller grid sizes lead to a lower spatial resolution (trapezoid) and worsen the diffusion for CFL numbers that are not equal to 1.

While the smooth squared sine wave is less prone to visual deviations, the square wave experiences a big impact for bad parameters. The accuracy analysis showed that this scheme is only first order accurate in time, but the derivation can also be used to find out how the dominant error takes shape. In fact, the lowest order terms of the truncation error included second order derivatives in time. Those are responsible for the diffusive behavior of the time evolution.

All in all, this numerical scheme successfully solves the linear advection equation for certain CFL numbers required for stability. Importantly, this scheme can only solve the equation for positive wave speeds, i.e. right moving waves, which greatly limits its use. Moreover, this algorithm is only accurate to first order in space and time which gives only minimal accuracy.

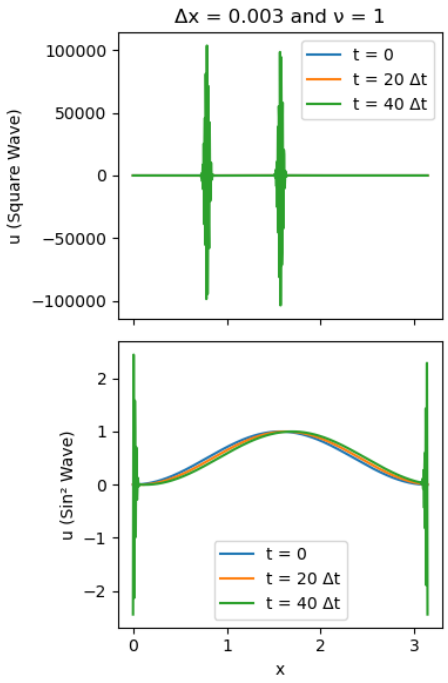

Figure 2. This figure shows the simulation domain for the FTCS scheme within several Δt's. Quickly, oscillations arise, that quickly lead to float overflows.

Forward Time Centered Space

The next algorithm, the Forward Time Centered Space scheme, uses the same approximation for the time derivative as above, but introduces a derivative in space that is centered around the point of interest. This promises and increase in spatial accuracy and could solve the directionality problem of the one-sided Euler derivatives.

$$\tilde{u}_j^{n+1} = u_j^n - \frac{a\Delta t}{2\Delta x}(u_{j+1}^n - u_{j-1}^n) \tag{7}$$

Although the accuracy analysis indeed shows that this algorithm increases the spatial accuracy compared to the FTBS scheme (see Eq. 15), the stability analysis also reveals that it is unconditionally unstable (see Eq. 16). This means it will always lead to numerically unstable solutions.

The numerical analysis shows this stability problem can even take effect on the first time step, depending on the steepness of the initial condition. Especially large slopes, like the square wave, will lead to instant oscillations, but also the smooth sine wave loses stability within fractions of a period.

Lax-Friedrichs

In a quest to overcome the stability problems, but still be able to harvest the advantages of a space centered scheme, the Lax-Friedrichs method expands the FTCS scheme by averaging the current function value spatially inside the time derivative.

$$\tilde{u}_j^{n+1} = \frac{1}{2}(u_{j+1}^n + u_{j-1}^n) - \frac{a\Delta t}{2\Delta x}(u_{j+1}^n - u_{j-1}^n) \tag{8}$$

Analytically, this leads to a stable solution as long as the absolute value of the CFL number remains smaller or equal to one (see Eq. 18). At the same time, the accuracy remains of first order in time but reduces to $\frac{\Delta x^2}{\Delta t}$ in space. Like the FTCS algorithm, this lowest order term features the second order derivative, i.e. a diffusive term. For —CFL— = 1, the amount of diffusion is identical to the FTCS scheme. However, for CFL numbers smaller than 1, $\Delta t < \Delta x$, so the magnitude of the diffusion error term is higher compared to FTCS.

The simulations agree with the analytical results, the numerical scheme regains stability, to the price of an added diffusion term. The plots look very similar to the FTCS plots otherwise (see attached).

Lax-Wendroff

Building on the achievements of the Lax-Friedrichs algorithm, the Lax-Wendroff scheme deliberately introduces an additional diffusive term to counteract the instability of the centered space difference.

$$\tilde{u}_j^{n+1} = u_j^n - \frac{a\Delta t}{2\Delta x}(u_{j+1}^n - u_{j-1}^n) \tag{9}$$

$$+ \frac{a^2\Delta t^2}{2\Delta x^2}(u_{j+1}^n - 2u_j^n + u_{j-1}^n) \tag{10}$$

This formulation achieves second order accuracy in time and space and is thus the most widely used method to solve linear equations. A stability analysis shows that this increase in temporal and spatial order in comparison to the Lax-Friedrichs algorithm comes at no expense for the stability. In fact, it remains at the best possible requirement for explicit finite difference schemes ($\nu \leq 1$).

The analysis of the simulation plot shows that instead of a predominantly diffusive behavior, the domain exhibits a mainly dispersive behavior. This is triggered by the 3rd order derivative being the smallest residual term. This odd derivative is responsible for the dispersion that again especially affects the edges of the square wave. In Fourier space, the square wave holds a lot of high frequency components, that are affected most by the phase shifts induced through dispersion. This is why most of the induced oscillations are visible here.

Looking at Figure 3, the dispersive behavior is highly affecting all square wave propagations for CFL numbers that are smaller than 1. The smooth sine wave, however, keeps its shape very well, even for parameter combination that showed a lot of amplitude damping for the other algorithms. However, for the combination of the smallest

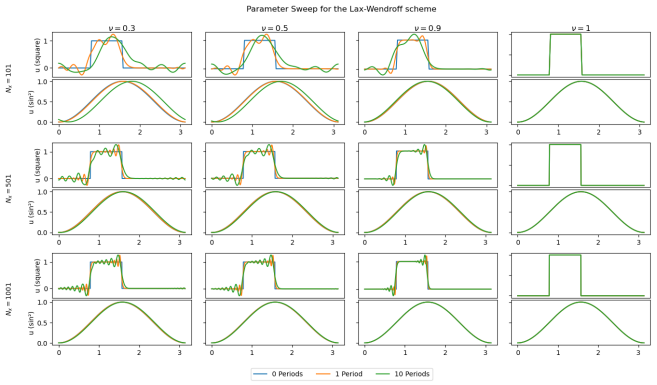

Figure 3. This figure shows the numerical behavior of the simulation domain for the Lax-Wendroff scheme. It shows the solutions over time and for different combinations of N_x and ν.

values for both parameters, the phase shifting behavior of the dispersive error results in a very visible translation of the squared sine wave.

Runge Kutta (2nd order) and CFD (4th order)

The combination of advanced two-step algorithm of the time derivative and a high (4th) order centered space difference is chosen to emphasize the inherent instability of all centered difference schemes. Without appropriate counteraction, these methods lead to instability on the promise of higher spatial resolution.

$$\begin{aligned}
\frac{\partial u}{\partial x} &= \frac{-u^n_{j+2} + 8u^n_{j+1} - 8u^n_{j-1} + u^n_{j-2}}{12\Delta x} \\
k_1 &= \frac{\partial u}{\partial t} = -a\frac{\partial u}{\partial x} \\
u^* &= u + \Delta t\, k_1 \\
k_2 &= \frac{\partial u^*}{\partial t} = -a\frac{\partial u^*}{\partial x} \\
\tilde{u}^{n+1}_j &= u^n_j + \tfrac{\Delta t}{2}\Big(k_1 + k_2\Big)
\end{aligned}$$

Runge-Kutta of second order works by first taking the slope at time n. Then, it extrapolates the function value to time $n+1$ (with the previously determined slope) and also determines the slope at this new position. Those two slopes are averaged and used to move forward in time. This leads to second order accuracy in time. For the higher order central difference scheme, the coefficients of the four positions to the left and right of the current position are determined such that all but the first derivative cancel to a desired order. This leads to fourth order accuracy in space.

However, this combination of approximations for the time and space derivative still leads to unconditionally unstable behavior. In fact, the numerical solution experiences oscillations almost identical to the ones described for the FTCS scheme.

Summary

All in all, two numerical schemes (FTCS and RK) are found to be unconditionally unstable and can therefore not be used for numerical simulations. FTBS presents itself as the simplest of all algorithms, also resulting in the lowest accuracy. Moreover, it has the disadvantage of only being suitable for one-sided wave propagation. LF expands the FTCS method such that an additional second-order term ensures stability at the expense of spatial resolution and induced diffusion. Lastly, LW optimizes the scheme to gain the highest (2nd order) accuracy in time and space. As a drawback, the lowest order error term is dispersive which leads to oscillations for wave forms featuring high wave numbers (e.g. steep slopes).

Table I. Summary of accuracy and stability results for all schemes.

Scheme	LTE order	Stability bound
FTCS	$\mathcal{O}(\Delta t, \Delta x)$	$0 \leq \nu \leq 1$
FTCS	$\mathcal{O}(\Delta t, \Delta x^2)$	*none* (uncond. unstable)
Lax-Friedrichs	$\mathcal{O}(\Delta t, \Delta x^2)$	$\lvert\nu\rvert \leq 1$
Lax-Wendroff	$\mathcal{O}(\Delta t^2, \Delta x^2)$	$\lvert\nu\rvert \leq 1$
RK2 & CFD4	$\mathcal{O}(\Delta t^2, \Delta x^4)$	*none* (uncond. unstable)

Although the LW scheme has the highest accuracy, it is worse in handling steep slopes compared to the LF method. For this reason, the Lax-Friedrichs algorithm is chosen for the numerical simulation of the Brio-Wu shock problem that prominently features steep slopes.

EXPANSION TO MHD

Outgoing from the numerical insight that was gained in the previous section, the Lax-Friedrichs algorithm will now be applied to solve the Brio-Wu shock problem outlined in [1]. For this problem, a one dimensional tube is initialized with a jump discontinuity between two different steady states in the middle of the cavity. At the left and right boundary these states are kept fixed, while the rest of the domain is evolved using the two-dimensional MHD equations. After simulation over a long time interval, the different dominant waves freeze into the domain, producing characteristic structures that are compared to the above-given reference.

$$\frac{\partial Q}{\partial t} + \frac{\partial F}{\partial x} = 0 \tag{11}$$

For this simulation, the spatial flux F is different from the state vector Q, so that the time and space derivative are parameterized with different functions. However, $F(Q)$,

so for every step, the flux is calculated from the state vector. This relationship of F and Q can be derived by bringing the MHD equations into their conservative form and expressing the flux in terms of the components of the state vector.

$$Q = \begin{pmatrix} \rho \\ \rho u \\ \rho v \\ B_x \\ B_y \\ e \end{pmatrix}, \qquad F(Q) = \begin{pmatrix} Q_2 \\ \frac{Q_2^2}{Q_1} + p(Q) + \frac{1}{2}\left(Q_5^2 - Q_4^2\right) \\ \frac{Q_2 Q_3}{Q_1} - Q_4 Q_5 \\ 0 \\ \frac{Q_2}{Q_1} Q_5 - \frac{Q_3}{Q_1} Q_4 \\ \left(Q_6 + p(Q) + \frac{1}{2}(Q_4^2 + Q_5^2)\right) \frac{Q_2}{Q_1} - Q_4 \left(\frac{Q_2}{Q_1} Q_4 + \frac{Q_3}{Q_1} Q_5\right) \end{pmatrix}. \tag{12}$$

Table II. Wave designations in the Brio-Wu shock tube solution.

Label	Type of Wave
FR	Fast Rarefaction
SM	Slow Magnetosonic Wave
C	Contact Discontinuity
SS	Slow Shock

Unlike in the previous section, the boundary conditions here are not periodic, but fixed to the initial state. Numerically, the simulation domain is expanded by the boundary conditions on both sides, so that the first and last point of the domain have a cell to the left and right of them respectively. This is required for the LF algorithm that uses the neighboring cells for its centered space difference.

The simulation domain is initialized with a discontinuity in the center of the cavity. This means there is an initial left and an initial right constant state that is in contact right in the middle of the cavity. From this, the eigenmodes (waves) travel outwards with their respective wave speeds and split up into distinctive wave fronts. Because of the self-similar nature of hyperbolic systems, the waves freeze into place over time, revealing the characteristic structures.

At this point it should be mentioned that the applied case differs a lot from the simplest linear form discussed in the section above, with regard to the wave speed. Above, the equation only features one characteristic wave speed, so the CFL number can easily be chosen to be equal to one for all times t. Here, however, the system has multiple characteristic wave speeds that are additionally dependent on the current state of the system. This means the CFL number changes constantly and cannot simply be set to 1 in the beginning. Even worse, the time step size has to be chosen such that the CFL number will always fulfill $|\nu| \leq 1$ to avoid instability. Alternatively, a variable time step size could be added to always ensure that the CFL number remains at 1, possibly enhancing the quality of the result. A danger of this method is that for increasing wave speeds the time step size becomes smaller and smaller, basically stalling the simulation.

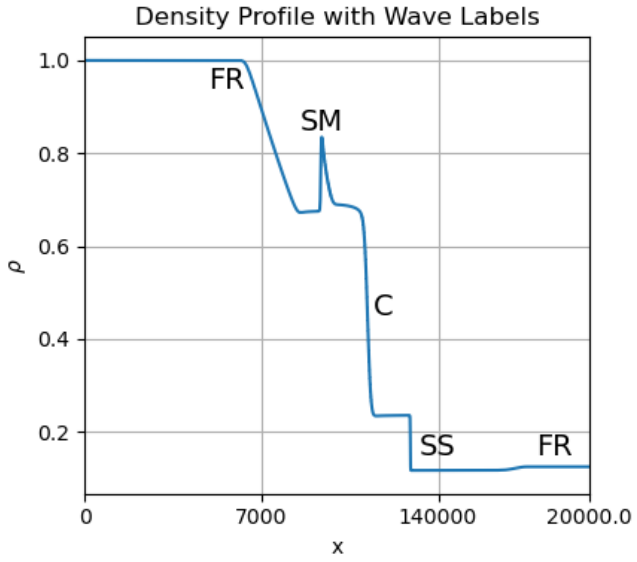

Figure 4. Here, the density profile of a 20,000 point large simulation domain after evolution over 10,000 time steps with the LF algorithm is depicted. The capitalized letters tag the kind of waves that are present in this cavity, after an initial Riemann discontinuity in the middle of the simulation domain.

Comparing Figure 4 and 5 to Figure 5 in [1], shows that the numerical solution was exactly matched by this simulation. The conducted simulation shows all characteristic wave forms that are indicated on the Figures and tabulated in Table II.

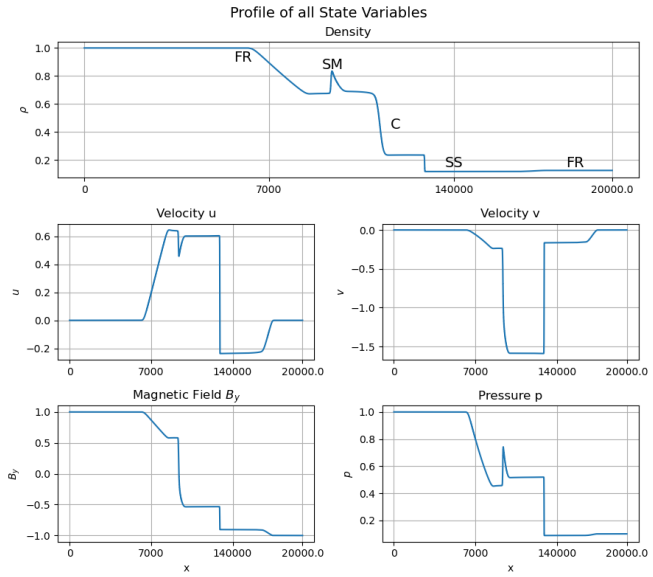

Figure 5. On this graphic, all state variables are plotted throughout the cavity. This shows how different kind of waves exhibit different behavior across the state variables.

CONCLUSION

This study compared five explicit Finite Difference Methods for the linear advection equation under periodic boundary conditions. Analytic accuracy and stability analysis (summarized in Table I) revealed a clear hierarchy: FTCS and the high-order RK method are unconditionally unstable and therefore useless, FTBS and LF are only first-order accurate in time but conditionally stable, and LW achieves second-order accuracy in both space and time while retaining the optimal stability bound $|\nu| \leq 1$.

Numerical experiments confirmed the error analysis that diffusive errors dominate the FTCS and LF scheme, while dispersive ones characterize the LW simulations. Furthermore, all centered space schemes without additional damping got lost in numerical instability. Selecting $\nu = 1$ minimized the error for the stable methods and largely preserved waveform integrity over ten periods.

In the following, the most robust scheme regarding sharp discontinuities (Lax-Friedrichs) was extended to solve the ideal-MHD system. The simulation reproduced the Brio-Wu reference solution and thereby demonstrated the applicability of the discussed schemes to real physical problems. The small simulation runtimes also showed the advantage simple numerical algorithms have regarding scalability.

[1] M. Brio and C. C. Wu, An Upwind Differencing Scheme for the Equations of Ideal Magnetohydrodynamics, Journal of Computational Physics **75**, 400 (1988).

Accuracy and Stability Analysis

Definitions

$$u \equiv u_j^n, \qquad u_t \equiv \frac{\partial u}{\partial t}\Big|_j^n, \quad u_{tt} \equiv \frac{\partial^2 u}{\partial t^2}\Big|_j^n,$$
$$u_x \equiv \frac{\partial u}{\partial x}\Big|_j^n, \quad u_{xx} \equiv \frac{\partial^2 u}{\partial x^2}\Big|_j^n, \quad \dots$$

1. Forward Time, Backward Space (FTBS)

Accuracy

$$\begin{aligned}
\tilde{u}_j^{n+1} &= u_j^n - \nu\big(u_j^n - u_{j-1}^n\big) \\
&= u - \nu\Big(u - u + \Delta x\, u_x - \tfrac{\Delta x^2}{2}\, u_{xx}\Big) \\
&= u - a\Delta t\, u_x + \tfrac{a\Delta x\Delta t}{2}\, u_{xx} \\
&= u + \Delta t\, u_t + \tfrac{\Delta x\,\Delta t}{2a}\, u_{tt} + \mathcal{O}\big(\Delta x^3\big) \\
\tau &= (u_j^{n+1} - \tilde{u}_j^{n+1})/\Delta t \\
&= \tfrac{\Delta t}{2}\, u_{tt} - \tfrac{\Delta x}{2a}\, u_{tt} + \mathcal{O}\big(\Delta t^2, \Delta x^2\big) \\
&\to \text{ Accuracy } \mathcal{O}\big(\Delta t, \Delta x\big)
\end{aligned} \tag{13}$$

Stability

$$\begin{aligned}
\varepsilon_j^{n+1} &= \varepsilon_j^n - \nu\big(\varepsilon_j^n - \varepsilon_{j-1}^n\big) \\
V^{n+1} e^{ikjx} &= V^n e^{ikjx} - V^n e^{ikjx} \nu\big(1 - e^{-i\theta}\big) \\
\tfrac{V^{n+1}}{V^n} &= 1 - \nu + \nu(\cos\theta - i\sin\theta) \\
|G|^2 &= 1 - 2\nu(1-\nu)(1-\cos\theta) \le 1 \\
&\to\ 0 \le \nu \le 1 \quad \forall\ \ \theta = k\Delta x
\end{aligned} \tag{14}$$

2. Forward Time, Centered Space (FTCS)

$$\begin{aligned}
\tilde{u}_j^{n+1} &= u_j^n - \tfrac{\nu}{2}\big(u_{j+1}^n - u_{j-1}^n\big) \\
&= u - \tfrac{\nu}{2}\Big(\big[u + \Delta x\, u_x + \tfrac{\Delta x^2}{2} u_{xx} + \tfrac{\Delta x^3}{6} u_{xxx}\big] \\
&\qquad - \big[u - \Delta x\, u_x + \tfrac{\Delta x^2}{2} u_{xx} - \tfrac{\Delta x^3}{6} u_{xxx}\big]\Big) \\
&= u - \nu\Big(\Delta x\, u_x + \tfrac{\Delta x^3}{6} u_{xxx}\Big) \\
&= u + \Delta t\, u_t + \tfrac{\Delta t\,\Delta x^2}{6a^2}\, u_{ttt} + \mathcal{O}\big(\Delta x^4\big), \\
\tau &= (u_j^{n+1} - \tilde{u}_j^{n+1})/\Delta t \\
&= \tfrac{\Delta t}{2}\, u_{tt} - \tfrac{\Delta x^2}{6a^2}\, u_{tt} + \mathcal{O}\big(\Delta t^2, \Delta x^3\big) \\
&\to \text{ Accuracy } \mathcal{O}\big(\Delta t, \Delta x^2\big)
\end{aligned} \tag{15}$$

Stability

$$\begin{aligned}
\varepsilon_j^{n+1} &= \varepsilon_j^n - \tfrac{\nu}{2}\big(\varepsilon_{j+1}^n - \varepsilon_{j-1}^n\big) \\
V^{n+1} e^{ikjx} &= V^n e^{ikjx} - \tfrac{\nu}{2} V^n e^{ikjx}\big(e^{i\theta} - e^{-i\theta}\big) \\
\tfrac{V^{n+1}}{V^n} &= 1 - i\nu\sin\theta \\
|G|^2 &= 1 + \nu^2 \sin^2\theta > 1 \\
&\to \text{ unstable} \quad \forall\ \ \theta = k\Delta x,\ \nu \ne 0
\end{aligned} \tag{16}$$

3. Lax–Friedrichs

$$\begin{aligned}
\tilde{u}_j^{n+1} &= \tfrac{1}{2}\big(u_{j+1}^n + u_{j-1}^n\big) - \tfrac{\nu}{2}\big(u_{j+1}^n - u_{j-1}^n\big) \\
&= \tfrac{1}{2}\Big[u + \Delta x\, u_x + \tfrac{\Delta x^2}{2} u_{xx} + \tfrac{\Delta x^3}{6} u_{xxx}\Big] \\
&\quad + \tfrac{1}{2}\Big[u - \Delta x\, u_x + \tfrac{\Delta x^2}{2} u_{xx} - \tfrac{\Delta x^3}{6} u_{xxx}\Big] \\
&\quad - \nu\Big(\Delta x\, u_x + \tfrac{\Delta x^3}{6} u_{xxx}\Big) \\
&= u + \tfrac{\Delta x^2}{2}\, u_{xx} - \nu\Delta x\, u_x - \tfrac{\nu\Delta x^3}{6}\, u_{xxx} + \mathcal{O}(\Delta x^4) \\
&= u + \Delta t\, u_t + \tfrac{\Delta x^2}{2a^2}\, u_{tt} + \tfrac{\Delta t\,\Delta x^2}{6a^2}\, u_{ttt} + \mathcal{O}(\Delta x^4), \\
\tau &= (u_j^{n+1} - \tilde{u}_j^{n+1})/\Delta t \\
&= \tfrac{\Delta t}{2}\, u_{tt} - \tfrac{\Delta x^2}{2a^2\Delta t}\, u_{tt} - \tfrac{\Delta x^2}{6a^2}\, u_{ttt} + \mathcal{O}\big(\Delta t^2, \Delta x^3\big) \\
&\to \text{ Accuracy } \mathcal{O}\big(\Delta t, \Delta x^2/\Delta t\big)
\end{aligned} \tag{17}$$

Stability

$$\begin{aligned}
\varepsilon_j^{n+1} &= \tfrac{1}{2}\big(\varepsilon_{j+1}^n + \varepsilon_{j-1}^n\big) - \tfrac{\nu}{2}\big(\varepsilon_{j+1}^n - \varepsilon_{j-1}^n\big) \\
V^{n+1} e^{ikjx} &= \tfrac{1}{2} V^n e^{ikjx}\big(e^{i\theta} + e^{-i\theta}\big) \\
&\qquad - \tfrac{\nu}{2} V^n e^{ikjx}\big(e^{i\theta} - e^{-i\theta}\big) \\
\tfrac{V^{n+1}}{V^n} &= \cos\theta - i\nu\sin\theta \\
|G|^2 &= \cos^2\theta + \nu^2\sin^2\theta \le 1 \\
&\to\ |\nu| \le 1 \quad \forall\ \ \theta = k\Delta x
\end{aligned} \tag{18}$$

4. Lax–Wendroff

$$\begin{aligned}
\tilde{u}_j^{n+1} &= u_j^n - \tfrac{\nu}{2}\big(u_{j+1}^n - u_{j-1}^n\big) \\
&\qquad + \tfrac{\nu^2}{2}\big(u_{j+1}^n - 2u_j^n + u_{j-1}^n\big) \\
&= u - \nu\Big(\Delta x\, u_x + \tfrac{\Delta x^3}{6} u_{xxx}\Big) \\
&\quad + \nu^2\Big(\tfrac{\Delta x^2}{2} u_{xx} + \tfrac{\Delta x^4}{24} u_{xxxx}\Big) + \mathcal{O}(\Delta x^5) \\
&= u + \Delta t\, u_t + \tfrac{\Delta t^2}{2}\, u_{tt} \\
&\quad + \tfrac{\Delta t\,\Delta x^2}{6a^2}\, u_{ttt} + \tfrac{\Delta t^2\,\Delta x^2}{24a^2}\, u_{tttt} + \mathcal{O}(\Delta x^5) \\
\tau &= (u_j^{n+1} - \tilde{u}_j^{n+1})/\Delta t \\
&= \tfrac{\Delta t^2}{6}\, u_{ttt} - \tfrac{\Delta x^2}{6a^2}\, u_{ttt} - \tfrac{\Delta t\,\Delta x^2}{24a^2}\, u_{tttt} \\
&\quad + \mathcal{O}\big(\Delta t^2, \Delta x^4\big) \\
&\to \text{ Accuracy } \mathcal{O}\big(\Delta t^2, \Delta x^2\big)
\end{aligned} \tag{19}$$

Stability

$$
\begin{aligned}
\varepsilon_j^{n+1} &= \varepsilon_j^n - \tfrac{\nu}{2}\big(\varepsilon_{j+1}^n - \varepsilon_{j-1}^n\big) \\
&\quad + \tfrac{\nu^2}{2}\big(\varepsilon_{j+1}^n - 2\varepsilon_j^n + \varepsilon_{j-1}^n\big) \\
V^{\,n+1}e^{ikjx} &= V^{\,n}e^{ikjx}\Big[1 - \tfrac{\nu}{2}\big(e^{i\theta} - e^{-i\theta}\big) \\
&\quad + \tfrac{\nu^2}{2}\big(e^{i\theta} - 2 + e^{-i\theta}\big)\Big] \\
\tfrac{V^{\,n+1}}{V^{\,n}} &= 1 - i\nu\sin\theta + \nu^2\big(\cos\theta - 1\big) \\
|G|^2 &= \big[1 - \nu^2\big(1-\cos\theta\big)\big]^2 + \nu^2\sin^2\theta \\
&= 1 + 4\nu^2\big(\nu^2 - 1\big)\sin^4\tfrac{\theta}{2} \le 1 \qquad \text{Stability} \\
&\to\ |\nu| \le 1 \qquad \forall\ \ \theta = k\Delta x
\end{aligned} \tag{20}
$$

$$
\begin{aligned}
\tau &= (u_j^{n+1} - \tilde{u}_j^{\,n+1})/\Delta t \\
&= \tfrac{\Delta t^2}{6}\,u_{ttt} + \tfrac{\Delta x^4}{30a^4}u_{t^5} + \tfrac{\Delta t\,\Delta x^4}{60a^4}u_{t^6} \\
&\quad + \mathcal{O}\big(\Delta t^3, \Delta x^5\big) \\
&\to\ \text{Accuracy}\ \mathcal{O}\big(\Delta t^2, \Delta x^4\big)
\end{aligned} \tag{21}
$$

5. Runge-Kutta 2nd Order + CFD 4th Order

$$
\begin{aligned}
k_1 &= u_t = -au_x = -a(u_x + \tfrac{\Delta x^4}{30}u_{x^5}) + \mathcal{O}(\Delta x^5) \\
u^* &= u + \Delta t\,k_1 \\
k_2 &= u_t^* = k_1 + \Delta t\,a^2(u_{xx} + \tfrac{\Delta x^4}{30}u_{x^6}) + \mathcal{O}(\Delta x^6) \\
\tilde{u}_j^{\,n+1} &= u_j^n + \tfrac{\Delta t}{2}\Big(k_1 + k_2\Big) \\
&= u + \tfrac{\Delta t}{2}\Big(-a(u_x + \tfrac{\Delta x^4}{30}u_{x^5}) - a(u_x + \tfrac{\Delta x^4}{30}u_{x^5}) \\
&\qquad + \Delta t\,a^2(u_{xx} + \tfrac{\Delta x^4}{30}u_{x^6}) + \mathcal{O}(\Delta x^5)\Big) \\
&= u - \Delta t a u_x - \tfrac{\Delta t\Delta x^4}{30}au_{x^5} + \tfrac{\Delta t^2}{2}a^2u_{xx} \\
&\quad + \tfrac{\Delta t^2\Delta x^4}{60}a^2u_{x^5} + \mathcal{O}(\Delta x^5) \\
&= u + \Delta t\,u_t + \tfrac{\Delta t^2}{2}\,u_{tt} + \tfrac{\Delta t\Delta x^4}{30a^4}u_{t^5} \\
&\quad \tfrac{\Delta t^2\,\Delta x^4}{60a^4}u_{t^6} + \mathcal{O}(\Delta x^5)
\end{aligned}
$$

$$
\begin{aligned}
\varepsilon_j^{n+1} &= \varepsilon_j^n - a\Delta t\tfrac{\partial\varepsilon_j^n}{\partial x} + \tfrac{a^2\Delta t^2}{2}\tfrac{\partial^2\varepsilon_j^n}{\partial^2 x} \\
\tfrac{\partial\varepsilon_j^n}{\partial x} &= \tfrac{-e^{i2\theta} + 8e^{i\theta} - 8e^{-i\theta} + e^{-i2\theta}}{12\Delta x} \\
&= i\beta\varepsilon_j^n \quad \text{with} \quad \beta = \tfrac{8(\sin\theta - \sin 2\theta)}{6\Delta x} \\
\tfrac{\partial^2\varepsilon_j^n}{\partial^2 x} &= -\beta^2\varepsilon_j^n \\
V^{n+1}e^{ikjx} &= V^n e^{ikjx}\Big[1 - ia\beta\Delta t - \tfrac{a^2\Delta t^2}{2}\beta^2\Big] \\
|G|^2 &= \Big(1 - \tfrac{a^2\Delta t^2\beta^2}{2}\Big)^2 + \Big(a\Delta t\beta\Big)^2 \\
|G|^2 &= 1 + \tfrac{a^4\beta^4\Delta t^4}{4} \le 1 \\
&\to\ \text{unconditionally unstable}
\end{aligned} \tag{22}
$$